Mapping Field-Scale Soil Moisture With L-Band Radiometer and Ground-Penetrating Radar Over Bare Soil

François Jonard, Lutz Weihermüller, Khan Zaib Jadoon, Mike Schwank, Harry Vereecken, and Sébastien Lambot

***Abstract*—Accurate estimates of surface soil moisture are essential in many research fields, including agriculture, hydrology, and meteorology. The objective of this study was to evaluate two remote-sensing methods for mapping the soil moisture of a bare soil, namely, L-band radiometry using brightness temperature and ground-penetrating radar (GPR) using surface reflection inversion. Invasive time-domain reflectometry (TDR) measurements were used as a reference. A field experiment was performed in which these three methods were used to map soil moisture after controlled heterogeneous irrigation that ensured a wide range of water content. The heterogeneous irrigation pattern was reasonably well reproduced by both remote-sensing techniques. However, significant differences in the absolute moisture values retrieved were observed. This discrepancy was attributed to different sensing depths and areas and different sensitivities to soil surface roughness. For GPR, the effect of roughness was excluded by operating at low frequencies (0.2–0.8 GHz) that were not sensitive to the field surface roughness. The root mean square (rms) error between soil moisture measured by GPR and TDR was 0.038 $m^3 \cdot m^{-3}$. For the radiometer, the rms error decreased from 0.062 (horizontal polarization) and 0.054 (vertical polarization) to 0.020 $m^3 \cdot m^{-3}$ (both polarizations) after accounting for roughness using an empirical model that required calibration with reference TDR measurements. Monte Carlo simulations showed that around 20% of the reference data were required to obtain a good roughness calibration for the entire field. It was concluded that relatively accurate measurements were possible with both methods, although accounting for surface roughness was essential for radiometry.**

***Index Terms*—Active and passive remote sensing, digital soil mapping, ground-penetrating radar (GPR), microwave radiometry, soil moisture, surface roughness.**

Manuscript received January 4, 2010; revised December 17, 2010; accepted January 30, 2011. Date of publication April 19, 2011; date of current version July 22, 2011. This work was supported in part by the German Research Foundation (DFG) in the frame of the Transregional Collaborative Research Centre 32 and in part by the Fonds National de la Recherche Scientifique (Belgium).

F. Jonard, L. Weihermüller, K. Z. Jadoon, and H. Vereecken are with Agrosphere (IBG-3), Institute of Bio- and Geosciences, Forschungszentrum Jülich GmbH, 52425 Jülich, Germany (e-mail: f.jonard@fz-juelich.de; l.weihermueller@fz-juelich.de; k.z.jadoon@fz-juelich.de; h.vereecken@fz-juelich.de).

M. Schwank is with the Section 5.1 "Geoecology and Geomorphology," German Research Center for Geosciences GFZ, 14473 Potsdam, Germany (e-mail: schwan@gfz-potsdam.de).

S. Lambot is with Agrosphere (IBG-3), Institute of Bio- and Geosciences, Forschungszentrum Jülich GmbH, 52425 Jülich, Germany, and also with the Earth and Life Institute, Université Catholique de Louvain, 1348 Louvain-la-Neuve, Belgium (e-mail: s.lambot@fz-juelich.de; sebastien.lambot@uclouvain.be).

Digital Object Identifier 10.1109/TGRS.2011.2114890

I. Introduction

SURFACE water content is a key variable for estimating water and energy fluxes at the land surface. Knowledge of the spatial distribution and dynamics of the soil water content is essential in agricultural, hydrological, meteorological, and climatological research and applications. Soil sampling, time-domain reflectometry (TDR), as well as neutron and capacitance probes, are common methods used to characterize soil water content at the point scale. In general, these techniques are restricted to small observation areas and are tedious and time consuming. Furthermore, these techniques may disturb the soil structure and may not allow repeated measurements at the same point. Finally, point measurements are not expected to be representative of the within-field variability or even average field moisture [1].

Airborne and spaceborne remote-sensing techniques with either passive microwave radiometry or active radar instruments are the most promising methods for mapping surface soil moisture over larger areas [2]–[5]. Active radar instruments, particularly synthetic aperture radar, can provide high-spatial-resolution data from space (10–100 m). However, the radar signal is highly sensitive to the geometric structure of the soil surface [6]. To account for roughness effects, empirical radar scattering models have been developed by several authors [7]–[9], but all these models require site-specific calibrations [10]. Currently, no widely applicable radar model accounting for roughness effects is able to provide soil-moisture estimations at accuracies that would satisfy typical hydrological application requirements [5]. In addition, remote-sensing radar measurements are greatly affected by vegetation [3]. Active systems are therefore limited to flat areas with bare soils or low vegetation. On the other hand, numerous studies have also demonstrated the potential of passive microwave remote sensing to retrieve geophysical parameters such as soil moisture [5], [11]–[14]. Passive methods provide coarser spatial resolution data ($>$ 10 km) but are less influenced by surface roughness and vegetation cover [3]. Microwave radiometry in the L-band (1–2 GHz) is a promising technique to estimate soil moisture and has the advantage of being unaffected by cloud cover and independent of solar radiation [15], which allows all-weather and continuous (day and night) observations. The frequency band 1.400–1.427 GHz is a protected radio astronomy band, thus reducing radiometric measurement errors due to radio frequency interferences. Additionally, at these wavelengths ($\sim$21 cm), the soil emission depth is relatively large and the vegetation canopies are semitransparent [16], [17].

Few techniques are presently available to measure soil water content at an intermediate scale between the local and remote-sensing scales, namely, the field scale. However, they are particularly necessary for improving and validating large-scale remote-sensing data products [18]. In this respect, ground-penetrating radar (GPR) and ground-based microwave radiometry techniques are specifically suited for field-scale characterization.

Over the past decade, GPR technology has made significant progress and has shown great potential for mapping surface soil moisture at the field scale with high spatial resolution. Reviews on the use of GPR in soil and hydrological sciences are given by Huisman *et al.* [4] and Annan [19]. As the dielectric properties of water outweigh those of other soil components, the spatial distribution of water decisively controls GPR wave propagation in the subsurface. However, the forward model describing the radar backscatter measurements is usually subject to relatively strong simplifications with respect to electromagnetic wave propagation phenomena. This results in inherent errors in the water content retrieval, and moreover, this does not permit the exploitation of all the information contained in the radar data. To overcome this limitation, it is necessary to resort to full-waveform forward and inverse modeling of the GPR data, which has become the logical choice due to the computing resources now available [20]–[22]. Lambot *et al.* [23] proposed a full-waveform forward and inverse modeling approach, which particularly applies to off-ground GPR. The electromagnetic model is based on a solution of the 3-D Maxwell equations for waves propagating in multilayered media and correctly accounts for antenna effects and antenna–soil interactions. The model was shown to accurately reproduce the radar measurements, and model inversion was successfully applied to identify and map surface soil moisture in the field [24], [25].

In the past, several experiments were performed using ground-based and airborne L-band radiometers to better understand the effects of vegetation cover [26]–[29], soil temperature [30], [31], soil surface roughness [32], [33], snow cover [34], and topography [35] on the microwave emission from the Earth's surface. These effects have to be considered in the interpretation of the signatures measured; otherwise, soil-water-content retrieval becomes inaccurate. Algorithms for estimating surface soil moisture from passive data are available in the literature [36], [37]. These models include corrections for the surface roughness as well as for the vegetation cover and have been successfully applied in a wide range of conditions in ground-based and airborne experiments [3].

In this context, the further development of algorithms for soil-moisture retrievals based on passive and/or active remote-sensing techniques is essential to fully benefit from European Space Agency's Soil Moisture and Ocean Salinity mission launched in November 2009 and the National Aeronautics and Space Administration's upcoming Soil Moisture Active Passive (SMAP) mission scheduled for launch in 2014. For the proper calibration of such algorithms, ground-truth measurements collected at relevant scales are necessary. In this respect, both ground-based GPR and radiometer show great promise for mapping spatiotemporal variations of soil moisture at scales ranging from a few square meters to several hectares and with a spatial resolution on the order of 1 m [38]. These ground-based GPR and radiometer techniques overcome the limitations of the present ground truths (point information, see previous discussion) and constitute a promising solution for bridging the spatial scale gap between point information and large-scale remote-sensing data.

The objective of this paper is to compare L-band radiometer and off-ground ultra-wideband (UWB) GPR [23], [39] to map surface soil moisture at the field scale over bare soil. The effect of soil roughness on the passive microwave signal is also addressed by using an empirical roughness model. The uncertainty related to, respectively, radiometer, GPR, and TDR estimates is appraised and discussed by comparing the three characterization techniques, as absolute uncertainty quantification is relatively complex when dealing with unknown heterogeneities over different scales. In addition, Monte Carlo simulations were performed to evaluate the sensitivity of the roughness parameters with respect to the number of ground truths used for the model calibration, thereby providing valuable insights into the roughness calibration uncertainty. To the best of our knowledge, this study represents the first attempt to compare field-scale maps of soil moisture over a bare rough surface using radiometer and advanced GPR.

II. Materials and Methods

A. Experimental Setup

The experiment was conducted on July 14, 2009 on an agricultural field at the Selhausen test site of Forschungszentrum Jülich GmbH, Germany (longitude of 50° 87 N, latitude of 6° 45 E, and elevation of 105 m above sea level). The measurements were performed three months after the last plowing event on a compacted bare soil. The test site has a maximum inclination of 4° in the east–west direction. The ground water depth shows seasonal fluctuations between 3 and 5 m below the surface. The soil type is a Haplic Luvisol developed in silt loam according to the U.S. Department of Agriculture textural classification. In the upper horizons of the soil (0–30 cm), the grain-size distribution is largely dominated by the silt fraction (mean value of 65.0%). The mean clay and sand contents are 14.9% and 20.1%, respectively. In the upper part of the field, stones are observed. Due to the geomorphology and soil texture variation (around 5% within the experimental plot), a large natural variability in surface soil water content is present (around 0.10 $\mathrm{cm}^3 \cdot \mathrm{cm}^{-3}$) [24].

GPR, radiometer, and TDR data were collected on a $72 \times 16\ \mathrm{m}^2$ experimental plot located in the upper part of the test site (Fig. 1). This plot consists of eight transects, each consisting of 18 measurement points (measurement spacing: 2 and 4 m in the x- and y-direction, respectively). In order to produce a wide range of water contents, the plot was partially irrigated with different quantities of water in two different areas using a fire hose one day before the experiment. Fig. 1 shows the location of the irrigated area. The dark-gray area was irrigated with approximately $8\,\mathrm{l} \cdot \mathrm{m}^{-2}$, while the light-gray area was irrigated with approximately $4\,\mathrm{l} \cdot \mathrm{m}^{-2}$.

Measurements were performed with a radiometer and a GPR mounted on the back of a truck (see Fig. 2). The truck moved

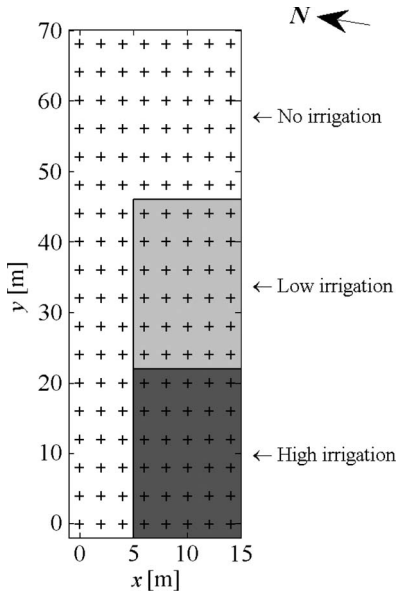

Fig. 1. Sampling grid (72×16 m^2) consisting of eight transects, each comprising 18 measurement points (in total 144 measurement points). The delineated areas correspond to areas with different levels of irrigation: (Dark gray) $\cong 8\,\mathrm{l} \cdot \mathrm{m}^{-2}$ (high irrigation), (light gray) $\cong 4\,\mathrm{l} \cdot \mathrm{m}^{-2}$ (low irrigation), and (white) $\cong 0\,\mathrm{l} \cdot \mathrm{m}^{-2}$ (no irrigation).

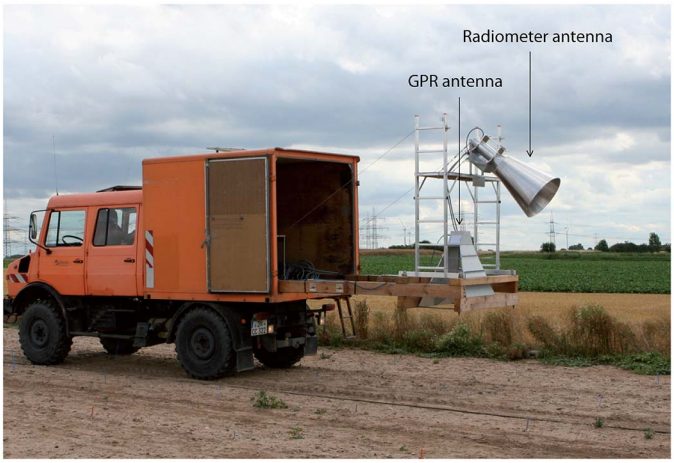

Fig. 2. GPR and L-band radiometer mounted on a truck to measure surface soil relative dielectric permittivity.

backward to avoid the effects of the tracks on the radiometer and radar measurements. Single radiometer and radar measurements were performed at each position. The radiometer antenna aperture was situated about 2 m above the soil surface and directed with an observation angle of $\vartheta = 53^\circ$ relative to the vertical direction. The GPR antenna aperture was about 1.2 m above the ground with normal incidence. This setup resulted in an elliptic -3-dB footprint of approximately 3.2×1.9 m^2 for the radiometer and a -3-dB footprint of approximately 1.8×1.8 m^2 for the GPR (see Sections II-C1 and II-C2).

B. Ground-Truth Measurements

Subsequent to each GPR and radiometer measurement, four TDR and temperature measurements were performed in the center of the GPR and the radiometer antenna footprints, at distances of about 20 cm from each other. Only four measurements were collected due to a time constraint during the mapping experiment, particularly to avoid significant temporal variations of surface soil moisture (evaporation). Data measured within each footprint were averaged for comparison with the permittivities derived from the GPR and radiometer. TDR measurements of ε_r were performed using a custom-made three-rod probe with a length of 10 cm which was inserted vertically into the soil. The TDR probe was connected to a TDR100 cable tester (Campbell Scientific, Logan, UT). The raw data of the waveform were stored and automatically analyzed by the commonly used tangent method in the time domain [40]. Due to the low clay content of the soil at the site, the frequencies of the TDR measurements are expected to be in the frequency range of 200–1000 MHz [41], which is similar to the GPR bandwidth. Soil temperature measurements were performed using a temperature sensor (Testo110, Testo Industrial Services, Lenzkirch, Germany) inserted vertically at a depth of 5 cm. This sensor provides the soil temperature with an accuracy of ± 0.2 K.

C. Remote-Sensing Instruments

1) GPR: The radar system was set up using a ZVL vector network analyzer (VNA, Rohde & Schwarz, Munich, Germany), thereby providing a UWB stepped-frequency continuous-wave radar. The antenna system consisted of a transverse-electromagnetic double-ridged broadband horn antenna (BBHA 9120 F, Schwarzbeck Mess-Elektronik, Schönau, Germany). The antenna was 95 cm long with a 68×96 cm^2 aperture area and a -3-dB full beamwidth in the E-plane and in the H-plane of 46° (at 400 MHz). The antenna nominal frequency range was 0.2–2 GHz, and its isotropic gain ranged from 9–14 dBi.

The raw GPR data consist of the frequency-dependent complex ratio S_{11} between the backscattered electromagnetic field and the incident electromagnetic field and were measured sequentially at 301 stepped operating frequencies over the range of 0.2–2 GHz with a frequency step of 6 MHz. Only lower frequency data (0.2–0.8 GHz), which were not affected by soil surface roughness according to Rayleigh's criterion ($h_c = \lambda/8$, where h_c is the critical height of the surface protuberances and λ is the wavelength), were used for the inversions.

2) Microwave Radiometer: The L-band microwave radiometer JÜLBARA from Forschungszentrum Jülich GmbH was designed for field-scale application in surface-soil-moisture experiments. JÜLBARA is a Dicke-type radiometer which operates at the central frequency of 1.414 GHz and is based on a similar concept (with respect to the filter characteristics and calibration sources) as the ELBARA radiometer [42]. To distinguish interferences from natural thermal radiance, the radiometer measured quasi-simultaneously at the two following frequency ranges: 1.400–1.414 and 1.414–1.427 GHz. The radiometer was equipped with a dual-mode conical horn antenna (aperture diameter $= 68$ cm, length $= 61$ cm) with symmetrical and identical beams and a -3-dB full beamwidth in the far field of 24°, which allowed the received radiance to be confined to a well-defined and narrow footprint area. The radiometer was equipped with internal cold (278 K) and hot (338 K) loads for calibration preceding each measurement. The measurements were recorded with 10-s integration time. The

estimated absolute accuracy of the radiometer was ± 1 K with a sensitivity better than 0.1 K. External calibration was done to correct for losses in the antenna cables and for noise generated by the physical temperature of the antenna and cables. This external calibration was performed by directing the radiometer toward the sky with an elevation angle of 60° above the horizon and by correcting the measured brightness temperature to the theoretical value as described by Pellarin *et al.* [43].

D. Signal Processing

1) GPR Full-Waveform Forward and Inverse Modeling: Assuming the distribution of the electromagnetic field measured by the antenna to be independent of the scatterer, i.e., only the phase and amplitude of the field change (plane-wave approximation over the antenna aperture), the antenna can be modeled using the following equation in the frequency domain, owing to the linearity of Maxwell's equations [23]

$$S_{11}(\omega) = H_i(\omega) + \frac{H(\omega)G^{\uparrow}_{\mathrm{xx}}(\omega)}{1 - H_f(\omega)G^{\uparrow}_{\mathrm{xx}}(\omega)} \tag{1}$$

where $S_{11}(\omega)$ is the international standard quantity measured by the VNA, $H_i(\omega)$ is the antenna return loss, $H(\omega)$ is the antenna transmitting–receiving transfer function ($H(\omega) = H_t(\omega)H_r(\omega)$), $H_f(\omega)$ is the antenna feedback loss, $G^{\uparrow}_{\mathrm{xx}}(\omega)$ is the transfer Green's function of the air and subsurface, and ω is the angular frequency. The antenna transfer functions and the Green's function are dimensionless. The characteristic antenna transfer functions can be determined by solving a system of equations as (1) to the unknowns $H_i(\omega)$, $H(\omega)$, and $H_f(\omega)$, by performing $S_{11}(\omega)$ measurements for known configurations, i.e., for which the Green's functions can be computed. Typically, $S_{11}(\omega)$ measurements are performed with the antenna at different heights above a perfect electrical conductor. The Green's function represents an exact solution of the 3-D Maxwell's equations for electromagnetic waves propagating in multilayered media with smooth interfaces [23], [44], [45].

In order to identify the surface dielectric permittivity, inversion of the Green's function is performed in the time domain, focusing on a time window containing the surface reflection only [39]. The inverse problem is formulated in the least squares sense, and the objective function to be minimized is accordingly defined as follows:

$$\phi(\mathbf{b}) = \left(\mathbf{g}^{\uparrow *}_{\mathrm{xx}} - \mathbf{g}^{\uparrow}_{\mathrm{xx}}\right)^{\mathrm{T}} \cdot \left(\mathbf{g}^{\uparrow *}_{\mathrm{xx}} - \mathbf{g}^{\uparrow}_{\mathrm{xx}}\right) \tag{2}$$

where

$$\mathbf{g}^{\uparrow *}_{\mathrm{xx}} = g^{\uparrow *}_{\mathrm{xx}}(t)\big|^{t_{\max}}_{t_{\min}} \quad \mathbf{g}^{\uparrow}_{\mathrm{xx}} = g^{\uparrow}_{\mathrm{xx}}(t)\big|^{t_{\max}}_{t_{\min}} \tag{3}$$

are the vectors containing the observed and simulated time domain windowed Green's functions, respectively, and $\mathbf{b} = [\varepsilon_r, h_a]$ is the parameter vector to be estimated with ε_r (dimensionless) being the surface soil relative dielectric permittivity and h_a (in meters) being the distance between the antenna phase center and the soil surface. The antenna phase center represents the origin of the radiated field from which the far-field spherical divergence is initiated [63]. Although the soil electrical conductivity, magnetic permeability, and soil layering can be taken into account in the inversion process, their effect was initially assumed to be negligible for the estimation of ε_r [39].

The objective function (2) is minimized using the local Levenberg–Marquardt algorithm. An initial guess for the antenna elevation h_a is derived from the surface reflection arrival time t_i (in seconds), which is automatically detected. Given the simple topography of the objective function (not oscillating and containing a single minimum) dealt with in this particular inverse problem, the initial guess for ε_r can be made arbitrarily, and it was set as 5 in this study (the solution found by the algorithm is independent of the initial guess). The GPR methodology has been fully validated in previous studies, both in the laboratory and in the field [23], [25], [39]. However, a validated UWB GPR model that accounts for soil surface roughness is not yet available [46].

2) Passive Microwave Signal Modeling:

a) Radiative transfer model: The basic principle of microwave radiometry is a measurement of the thermal radiance emitted at the Earth's surface in a given frequency band [15]. Planck's radiation law describes the radiation spectrum of a black body at a given physical temperature. At microwave frequencies, and for temperatures typical of the Earth's surface, Planck's law can be approximated by the Rayleigh–Jeans equation. According to this equation, the radiance is proportional to the physical temperature and is denoted as brightness temperature T_B (in kelvins) [15].

The brightness temperature of a soil surface observed by the L-band radiometer can then be expressed as [36], [47]

$$T_{B,p} = E_p T_{\mathrm{eff}} + (1 - E_p)T_{\mathrm{sky}} \tag{4}$$

where E (dimensionless) is the surface emissivity, T_{sky} (in kelvins) is the sky radiometric temperature calculated as in [43], T_{eff} (in kelvins) is the effective physical temperature of the soil [2], and p refers to the polarization [horizontal (H) or vertical (V)]. In this paper, the effective soil temperature is assumed to be the temperature at a depth of 5 cm. The impact of this assumption on the emissivity values is negligible. Indeed, even if an error of 5 K is assumed for T_{eff}, this would result in an error for the emissivity of less than 3%.

Under local thermodynamic equilibrum, Kirchhoff's law states that the emissivity (E) of a given object is equal to its absorptivity. The soil emissivity can then be related to the soil reflectivity R (dimensionless) by

$$E = 1 - R. \tag{5}$$

The reflectivity is described by the Fresnel equations that express the behavior of electromagnetic waves at a smooth dielectric boundary [48], [49]. By solving the Fresnel equations, ε_r of the emitting layer can be retrieved from the observed R at each polarization. However, the Fresnel equations are only valid for an ideal smooth air–soil interface which is never found in typical agricultural fields. To include the effects of roughness in the modeling of the microwave emission from soil surface, a simple model based on the semiempirical approach of Wang and Choudhury [50] was applied. This model is described next.

b) Roughness model: The Wang and Choudhury model [50] expresses the rough surface reflectivity $R_{R,p}(\vartheta)$ at a

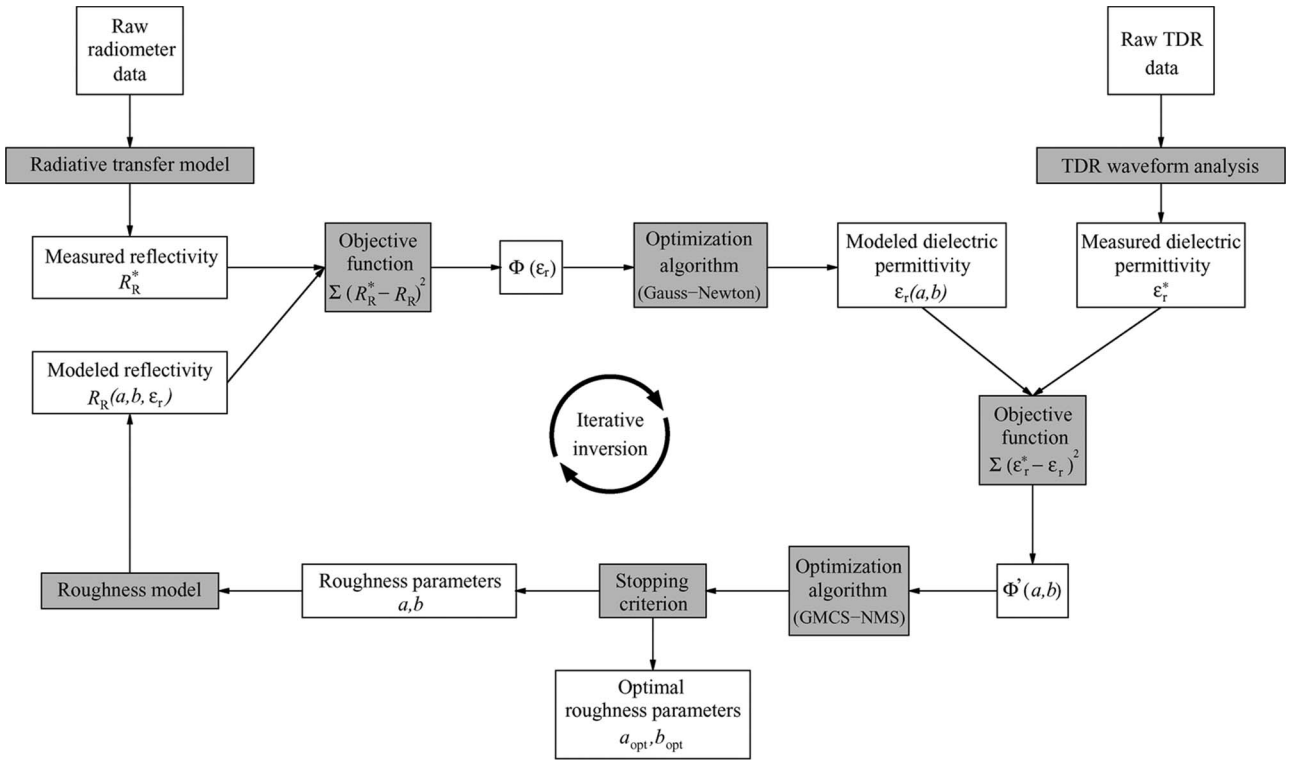

Fig. 3. Flowchart representing the calibration procedure for the roughness parameters a and b of (7) for estimating the soil relative dielectric permittivity. Shaded boxes denote operators, and white boxes denote variables.

polarization p (H or V) and an incidence angle ϑ in relation to the specular reflectivity $R_{F,p}(\vartheta)$ as

$$R_{R,p}(\vartheta) = [(1-Q)R_{F,p}(\vartheta) + QR_{F,p}(\vartheta)] \exp(-h\cos(\vartheta)^n) \tag{6}$$

where Q is the polarization mixing factor, n expresses the angular dependence of roughness, and h is the roughness parameter.

In our study, only a single incidence angle is used ($\vartheta = 53°$), and thus, the angular dependence of roughness will then not be considered ($n = 0$). In most studies, polarization crosstalk is assumed to be negligible, and thus, $Q = 0$ is used [47], [51]. In (6), the roughness parameter h is generally considered to be independent of polarization [47], [50]. However, various studies have pointed out that the roughness affects the two polarizations differently as a result of the anisotropy of the effective permittivity ε_r in the air to soil transition zone [52], [53]. Several studies have also shown that the roughness effect might change with soil moisture. Wigneron *et al.* [47], Schwank and Mätzler [54], and Escorihuela *et al.* [55] did indeed observe a negative correlation between their estimated roughness parameter and the surface soil moisture. The apparently increasing roughness with decreasing soil moisture was explained by an increase of the dielectric heterogeneity (dielectric roughness) as the soil dries out. However, a recent study by Escorihuela *et al.* [56] showed that the dependence of the soil roughness parameter on soil moisture is due to the difference between the L-band radiometer sensing depth and the ground-truth sampling depth used for the calibration. Based on these assumptions, a simplified bare soil reflectivity model accounting for roughness was derived

$$R_{R,p} = R_{F,p} \exp(-(a_p + b_p \varepsilon_r)) \tag{7}$$

where a and b are the soil roughness model parameters depending on polarization p. Parameter b is multiplied by ε_r instead of the volumetric soil water content to avoid any inaccuracy due to the petrophysical relationship. Given that the model parameters are determined by best fit, they include the measurements errors and their physical meaning is not straightforward [55].

The inversion procedure adopted for the estimation of the roughness parameters is shown in Fig. 3. In this optimization process, only radiometer and reference TDR data are used. Inversion is composed of two sequential optimization steps. The first inverse problem consists of solving a nonlinear least squares problem. In this case, the Gauss–Newton algorithm is used to minimize the objective function

$$\Phi(\varepsilon_r) = \sum (R_R^* - R_R)^2 . \tag{8}$$

This objective function represents the cumulative squared error between the measured and modeled reflectivity radiometer data (R_R^* and $R_R(a,b)$, respectively). The measured reflectivity data are obtained from the brightness temperature measurements by using the radiative transfer model presented in (4) and (5). The radiometer data from each polarization are used separately in the inversion procedure to obtain specific roughness parameters for each polarization. The second inverse problem consists in minimizing the objective function

$$\Phi'(a,b) = \sum (\varepsilon_r^* - \varepsilon_r)^2 . \tag{9}$$

The objective function Φ' represents the cumulative squared error between the measured and modeled dielectric permittivity data (ε_r^* and $\varepsilon_r(a,b)$, respectively) and is minimized by means of the global multilevel coordinate search optimization

algorithm combined with the local Nelder–Mead simplex algorithm (GMCS-NMS, see [57]). Measured permittivity data are obtained from raw TDR data while modeled permittivity data are obtained from the solutions of the first inverse problem. At each iteration, new roughness parameters are generated, which are used in the roughness model (7) to produce new modeled reflectivity data and then new modeled dielectric permittivity data. The optimal roughness parameters a and b are finally obtained after numerous iterations. For the optimization convergence criteria, the default values of the implementation of the Nelder–Mead simplex algorithm in Matlab (The MathWorks Inc.) were used (i.e., termination tolerance on the function value set to 10^{-4} and termination tolerance on the optimized parameters set to 10^{-4}). It has to be noted that more stringent conditions did not affect the fitting results.

E. Petrophysical Relationship

For each type of measurement (GPR, radiometer, and TDR), the model of Topp *et al.* [58] was used to relate the soil volumetric water content $[\theta\ (\text{in m}^3 \cdot \text{m}^{-3})]$ to the soil relative dielectric permittivity

$$\theta = -5.3 \times 10^{-2} + 2.92 \times 10^{-2}\varepsilon_r - 5.5 \times 10^{-4}\varepsilon_r^2 + 4.3 \times 10^{-6}\varepsilon_r^3. \quad (10)$$

The Topp model is a widely used empirical relationship mainly applied for TDR measurements with some restrictions for highly clayic- and organic-rich soils as well as soils with high bulk electrical conductivity. For our study site, Topp's model was shown to perform well by Weihermüller *et al.* [24]. The authors found a root-mean-square (rms) error of 0.021 $\text{m}^3 \cdot \text{m}^{-3}$ between volumetric soil samples and TDR estimates.

III. Results and Discussion

A. Off-Ground GPR

Fig. 4 shows the frequency- and time-domain GPR Green's functions for one and the 144 measurement points, respectively. The Green's function is computed from the S_{11} scatter function using (1), thereby filtering antenna effects. In the frequency domain, we observe that the amplitude of the Green's function $(G^{\uparrow}_{\text{xx}})$ increases monotonically up to approximately 0.8 GHz. This behavior indicates that the surface reflection dominates the radar backscatter (this corresponds to a single reflection in the time domain) [39]. For higher frequencies, $G^{\uparrow}_{\text{xx}}$ presents a highly oscillating behavior. This is to be attributed to the effect of soil surface roughness [46]. Indeed, for this particular radar setup, the frequency at which a surface appears to be smooth agrees with the Rayleigh criterion [59]. Accordingly, the critical height of the surface protuberances below which the soil surface can be considered smooth corresponds to one-eighth of the wavelength. In our case, the threshold frequency is around 0.8 GHz, corresponding to a maximum height of the surface protuberances of about 0.047 m, which is consistent with the conditions visually observed in the field. In the time domain [Fig. 4(b)], the Green's function $(g^{\uparrow}_{\text{xx}})$ does indeed present a single reflector (the soil surface). The time zero corresponds to the antenna

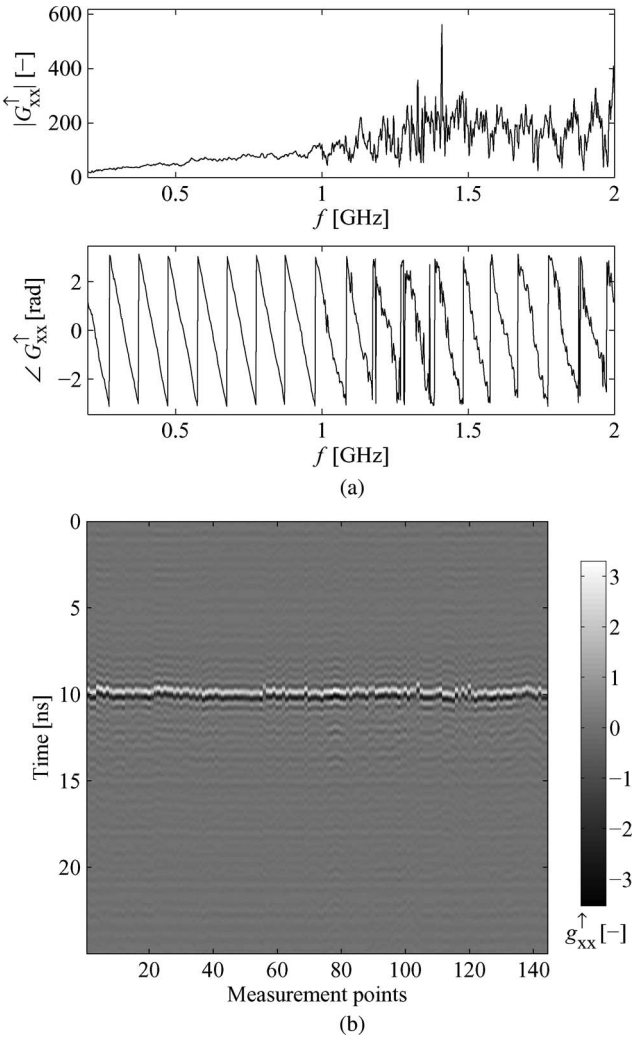

Fig. 4. Representation of the Green's function (a) in the frequency domain for one measurement point ($|G^{\uparrow}_{\text{xx}}|$ denotes the amplitude, and $\angle G^{\uparrow}_{\text{xx}}$ represents the phase of the Green's function) and (b) in the time domain for all measurement points. The oscillations observed with respect to time (above and below the reflection observed around 10 ns) are an artefact of the inverse Fourier transform when data are used in a limited frequency window.

phase center. The variations of the reflection over time are due to the inherent variations of the antenna height above the soil during the measurements. It is worth noting that the soil moisture retrieved from the reflection at the air–soil interface is a surface property and not a volume property (reflection coefficient) [39], [60]. Hence, the retrieved soil moisture does not directly depend on the penetration depth of the GPR electromagnetic waves. However, when dielectric contrasts are present near the soil surface, and in particular, at depths which are a fraction of the wavelength (typically less than a quarter the wavelength), constructive or destructive interferences occur and affect the results, leading to, respectively, over- or underestimations of soil surface dielectric permittivity [39], [60].

B. Soil-Moisture Maps

In the first step, off-ground GPR and radiometer data were analyzed without taking soil roughness into account. Surface soil moisture estimated from GPR (θ_{GPR}), radiometer (θ_{MR}),

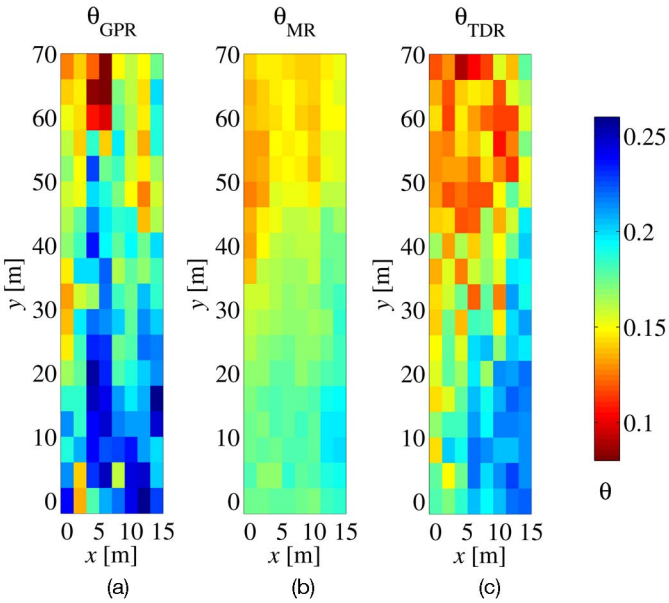

Fig. 5. Volumetric water content maps obtained using (a) off-ground GPR, (b) radiometer (averaged over both polarizations), and (c) TDR measurements at the Selhausen test site (July 14, 2009).

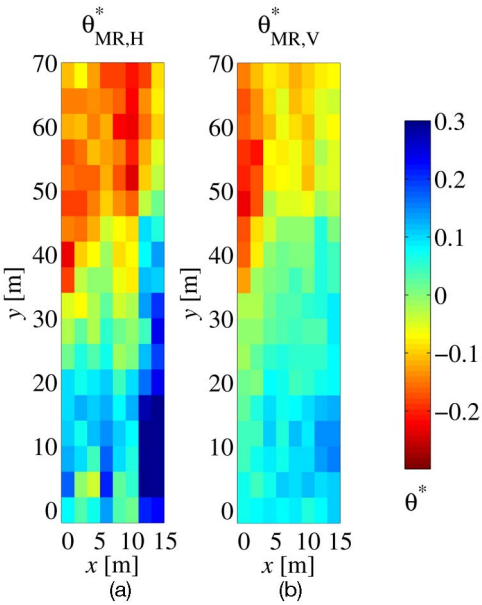

Fig. 6. Maps of the normalized water content (11) with respect to the spatially averaged water content obtained using the radiometer at (a) H and (b) V polarizations.

and TDR (θ_{TDR}) measurements are shown in Fig. 5. As expected, the soil-water-content map based on the GPR measurements [Fig. 5(a)] shows the lowest water contents in the upper part of the field, which was not irrigated. Intermediate water contents are observed in the area of low irrigation and highest water contents in the area of high irrigation (Fig. 1). Although the left part of the field was not irrigated, a water content gradient is detectable from the upper to the lower left part. This is associated with the slope of the field. GPR-derived water content values range between 0.12 and 0.26 $\mathrm{m}^3 \cdot \mathrm{m}^{-3}$.

In comparison to the GPR-derived water content map, the results of the radiometer measurements, considering the average between the horizontal (subscript H) and vertical (subscript V) polarizations ($\theta_{\mathrm{MR},\overline{\mathrm{HV}}}$) [Fig. 5(b)], show a smaller water content range (0.13–0.20 $\mathrm{m}^3 \cdot \mathrm{m}^{-3}$). However, a similar moisture pattern to that of GPR is observed with the lowest water contents in the upper nonirrigated area, intermediate water contents in the area of low irrigation, and the highest water contents in the area of high irrigation. Additionally, the spatial correlation is much higher compared with the GPR, with smoother transitions between drier and wetter parts. This may partly be attributed to the larger footprint of the radiometer and, as shown below, to the polarization averaging.

The map based on the reference TDR measurements [θ_{TDR}, Fig. 5(c)] shows the widest range of water contents over the entire field with values from 0.09 $\mathrm{m}^3 \cdot \mathrm{m}^{-3}$ in the upper nonirrigated area to a maximum of 0.23 $\mathrm{m}^3 \cdot \mathrm{m}^{-3}$ in the area of high irrigation. This is due to a significant local variability at the GPR and radiometer footprint scales, as observed from the repeated TDR measurements within the footprints (average standard deviation (STD) of 0.02 $\mathrm{m}^3 \cdot \mathrm{m}^{-3}$). It is also worth noting that TDR measurements were affected by the presence of numerous stones in the field, particularly in the upper part, thereby also leading to significant measurement errors (typically underestimations). Nevertheless, the same general moisture pattern as for the GPR and the radiometer is obtained.

As already stated previously, two polarizations were measured by the radiometer, namely, H and V. For the H polarization, water content values ($\theta_{\mathrm{MR,H}}$) range between 0.08 and 0.15 $\mathrm{m}^3 \cdot \mathrm{m}^{-3}$, and for the V polarization, the water content values ($\theta_{\mathrm{MR,V}}$) range between 0.16 and 0.25 $\mathrm{m}^3 \cdot \mathrm{m}^{-3}$ (data not shown). Radiometer measurements at H and V polarizations provide large differences in water content estimations in terms of absolute values. This discrepancy can be ascribed to the different sensitivities to the soil surface roughness with respect to the polarization. Indeed, Mo *et al.* [61] and Shi *et al.* [52] showed that roughness effects on the surface effective reflectivity differ at different polarizations for the same roughness characteristics. For both polarizations, Fig. 6 shows the corresponding normalized water content value ($\theta^*_{\mathrm{MR},p}$) defined as follows:

$$\theta^*_{\mathrm{MR},p} = \frac{\theta_{\mathrm{MR},p} - \overline{\theta_{\mathrm{MR},p}}}{\overline{\theta_{\mathrm{MR},p}}} \tag{11}$$

where $\overline{\theta_{\mathrm{MR},p}}$ is the water content estimated by the radiometer at polarization p and spatially averaged over the entire field. This shows that although the absolute water contents are under- or overestimated with the H and V polarizations, the spatial pattern is similar for the two normalized maps (correlation coefficient $r^2 = 0.74$) and consistent with the GPR and TDR maps (wetter and drier zones). The remaining differences between the two polarizations in the spatial distribution of the retrieved water content may be attributed to variations in soil roughness within the field, which are not fully removed by normalization (only the linear bias is removed).

C. Comparison of the Measurement Methods

For a direct comparison of the results obtained from the different measurement methods, the GPR- and radiometer-derived water contents are plotted with respect to the TDR

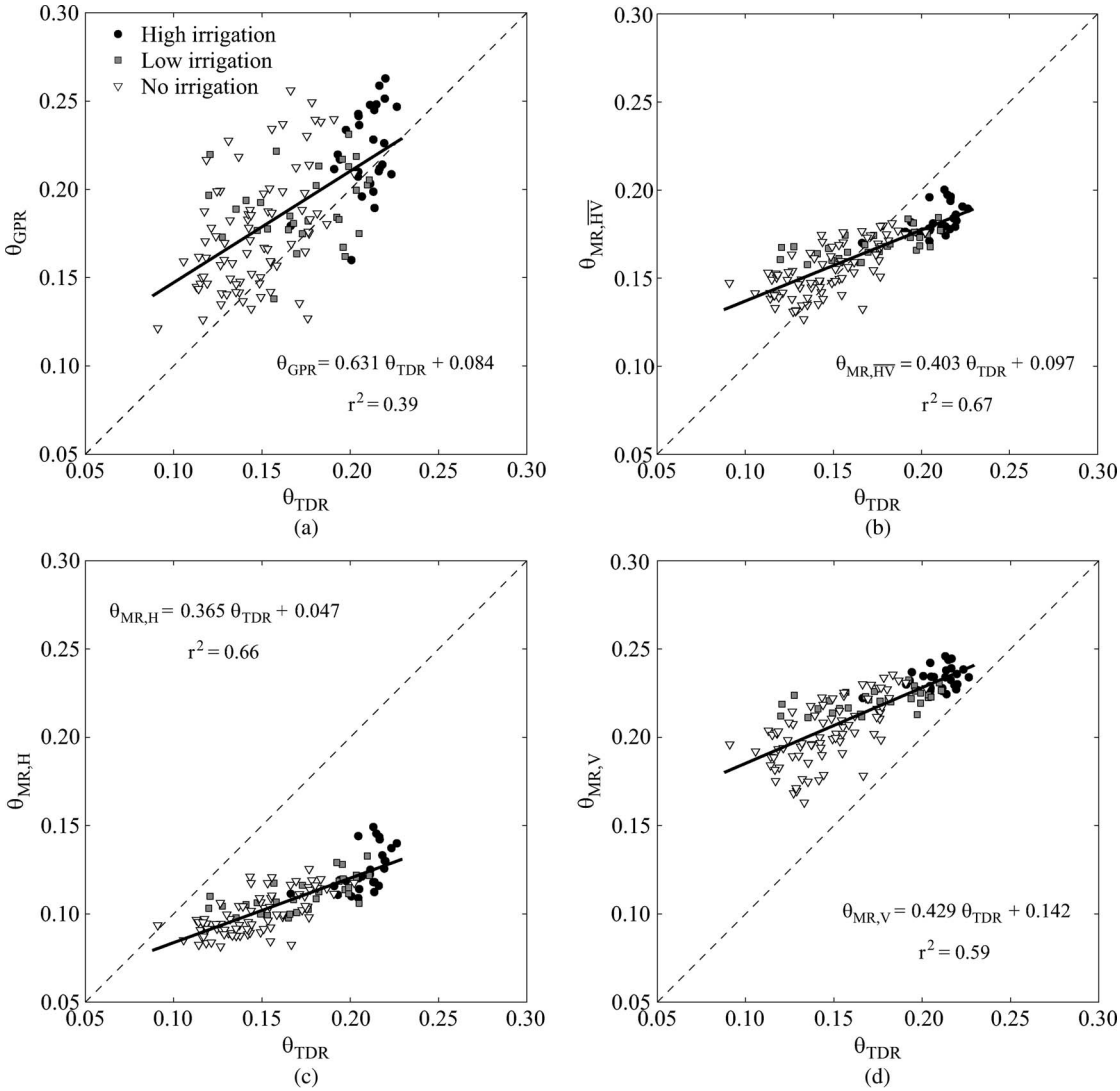

Fig. 7. Volumetric soil water content from (a) off-ground GPR versus TDR, (b) radiometer (averaged over both polarizations) versus TDR, (c) radiometer (H polarization) versus TDR, and (d) radiometer (V polarization) versus TDR.

results (Fig. 7). To facilitate interpretation, the data sets were divided into three classes, corresponding to the high (dark gray), low (light gray), and nonirrigated (white) parts, as shown in Fig. 1.

In Fig. 7(a), it can be observed that GPR-derived water contents systematically overestimate the TDR measurements. Additionally, the data points are highly scattered, resulting in a low correlation coefficient (r^2) of 0.39 and an rms error in terms of water content of 0.038 $\mathrm{m}^3 \cdot \mathrm{m}^{-3}$ (see Table I). The relatively large STD (0.029) observed for the GPR measurements with respect to the TDR reference measurements may be attributed to soil heterogeneity. In [23], laboratory results are presented for a quite homogeneous medium with two layers, and the STD is indeed much smaller (0.007). For field conditions, Lambot *et al.* [25] obtained an STD of 0.023. However, compared with the radiometer, the slope of the regression (0.63) is much closer to 1. The observed discrepancies are similar for the three differently irrigated areas of the field. The lower values for the TDR may be attributed to the difficulties encountered in properly inserting the TDR probe into the soil, particularly in the drier and stone-rich nonirrigated part of the field. This would explain the larger misfit of the regression line compared with the 1 : 1 line for lower water contents. It is also worth noting that the GPR measurements may be affected by dielectric layering near the soil surface, which may lead to constructive and destructive interferences, and, thereby, to over- or underestimations of the surface dielectric permittivity [60]. The soil apparent electrical conductivity (including dielectric losses) can also affect the GPR measurements. As showed by Lambot *et al.* [39], the effect of the soil electrical conductivity on the surface reflection and dielectric permittivity estimates is negligible for conductivity values below 0.03 $\mathrm{S} \cdot \mathrm{m}^{-1}$ which is larger than the apparent electrical conductivity observed in the field during the experiment $(< 0.025\ \mathrm{S} \cdot \mathrm{m}^{-1})$.

The comparison of averaged radiometer results (not accounting for roughness) and TDR data shown in Fig. 7(b) shows less scattering, with a higher r^2 of 0.67 and a lower rms error of 0.022 $\mathrm{m}^3 \cdot \mathrm{m}^{-3}$. The slope of the regression line is 0.4. Fig. 7(c) and (d) clearly show that the radiometer-derived water contents with H polarization significantly underestimate the TDR-derived values, while those with V polarization systematically lead to an overestimation. These discrepancies can be attributed

TABLE I
DIAGONAL MATRICES OF RMS ERROR IN TERMS OF WATER CONTENT (RMS ERROR θ) AND RELATIVE DIELECTRIC PERMITTIVITY (RMS ERROR ε_r) FOR THE GPR-, TDR-, AND RADIOMETER-AVERAGED ($\overline{\text{HV}}$-POL), HORIZONTAL (H-POL), AND VERTICAL (V-POL) POLARIZATIONS, RESPECTIVELY

	RMS error θ				RMS error ε_r			
	Radiometer $\overline{\text{HV}}$-pol	Radiometer H-pol	Radiometer V-pol	TDR	Radiometer $\overline{\text{HV}}$-pol	Radiometer H-pol	Radiometer V-pol	TDR
GPR	0.038	0.084	0.041	0.038	1.933	4.065	2.065	1.881
Radiometer $\overline{\text{HV}}$-pol		0.056	0.050	0.022		2.580	2.580	1.096
Radiometer H-pol			0.106	0.062			5.160	2.941
Radiometer V-pol				0.054				2.658

to the different sensitivities of the two polarizations with respect to roughness. In general, the H polarization better predicts the lower water contents in the nonirrigated areas compared with the higher water contents from the irrigated parts. Indeed, in Fig. 7(c), the low-water-content data are closer to the 1 : 1 line compared with the higher water content data, whereas the opposite is observed in Fig. 7(d). However, the r^2 is still 0.66 $m^3 \cdot m^{-3}$ for the H polarization and 0.59 $m^3 \cdot m^{-3}$ for the V polarization, respectively, whereby the high rms errors of 0.062 and 0.054 $m^3 \cdot m^{-3}$ clearly indicate the systematical mismatch between the two techniques. This explains the small rms error obtained by averaging the two polarizations.

The frequency dependence of the soil dielectric permittivity over the frequency range covered by the three methods (GPR, radiometer, and TDR) is expected to be rather small [23] as all methods operate at frequencies well below the relaxation frequency of free water (approximately 16 GHz). However, as the soil is inherently heterogeneous, differences in soil moisture retrieved by the three techniques can also be partly explained by the different characterized soil volumes.

D. Accounting for Soil Surface Roughness for the Radiometer

As already stated, soil surface roughness plays an important role in the retrieval of soil water content from the radiometer data. In this section, soil surface roughness is accounted for using the empirical roughness model [see (7)]. The optimal roughness parameters obtained by the inversion scheme in Fig. 3 are $a = 0.1818$ and $b = 0.0013$ for the H polarization and $a = -1.1480$ and $b = 0.0913$ for the V polarization, respectively. The value of b is close to zero for the H polarization, which means that the model dependence on ε_r is negligible for this polarization. It is worth noting that, as they are empirical, no constraint on the value of the estimated parameters during the inversion process was applied and their physical meaning is not straightforward. The values of these parameters depend on all electromagnetic phenomena that are not properly accounted for by the Fresnel model, particularly roughness effects, and measurement errors.

Fig. 8 shows the logarithm of the objective function $(\log_{10}(\phi'))$ as a function of the roughness parameters a and b. The aim of this analysis was to verify that the adopted optimization approach was able to find the global minimum of the parameter space correctly and accurately and also to analyze the uniqueness of the inverse solution and the parameter sensitivities, as well as the correlations between the two parameters. The objective function was calculated on 122 500 discrete points within the range $[-5 \leq a, b \leq 5]$ and shown in Fig. 8.

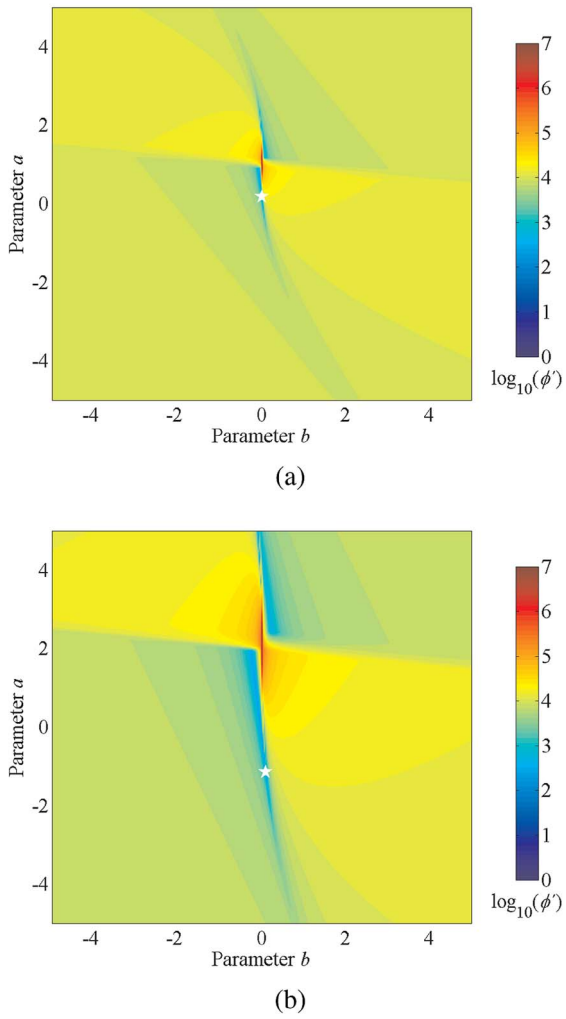

Fig. 8. Logarithm of the objective function $(\log_{10}(\phi'))$ as a function of the roughness parameters a and b. (a) H and (b) V polarizations. The star represents the global minimum of ϕ'. The optimal roughness parameters are $a = 0.1818$ and $b = 0.0013$ for the H polarization and $a = -1.1480$ and $b = 0.0913$ for the V polarization.

For both polarizations, the objective function shows a well-defined minimum (indicated by a white star), which is found by the global optimization procedure. The model is much less sensitive to a than to b, particularly for the V polarization, which may result in some uncertainty in the estimation of a.

Based on the optimal parameter values, the rms error between the TDR- and radiometer-derived (accounting for roughness) soil water contents is 0.020 $m^3 \cdot m^{-3}$ for both

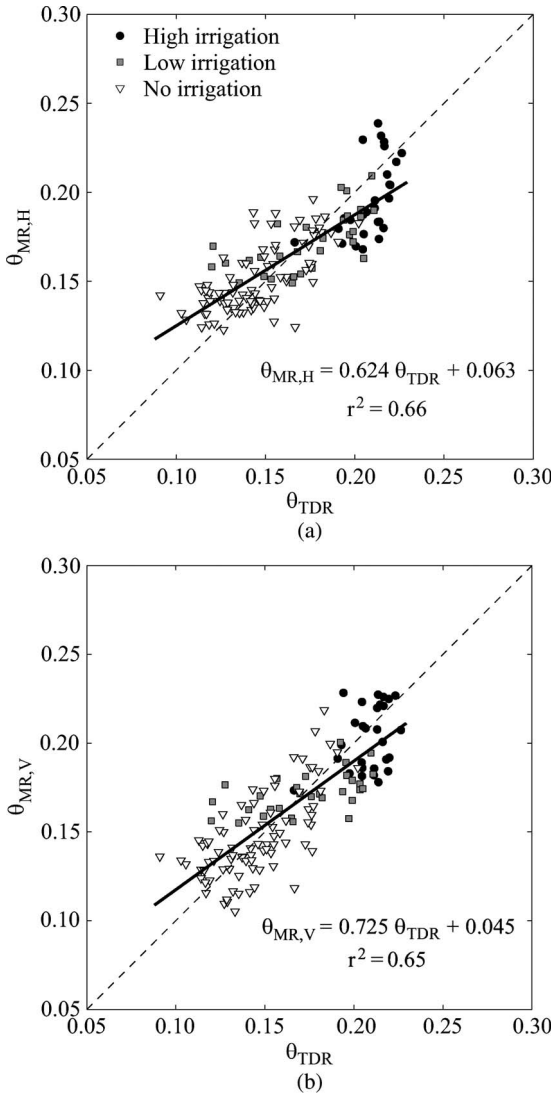

Fig. 9. Volumetric soil water content from (a) radiometer (H polarization) versus TDR and (b) radiometer (V polarization) versus TDR. Radiometer-derived water contents were estimated by taking roughness into account.

polarizations. In general, the accuracy of the soil-water-content retrieval is significantly improved by using the roughness model. In fact, the rms errors significantly decreased compared with those obtained without the roughness correction, namely, 0.062 and 0.054 $m^3 \cdot m^{-3}$ for the H and V polarizations, respectively (see Table I). The radiometer-derived water contents corrected for the roughness effect are plotted with respect to the TDR estimates in Fig. 9. Compared with Fig. 7(c) and (d), the measurements for both polarizations are much closer to the 1 : 1 line with a regression slope of 0.6 for the H polarization and 0.7 for the V polarization. Without the roughness correction, the regression slope was around 0.4 for both polarizations. However, the r^2 of the regression has not improved with the roughness model and the data scattering is similar. This means that random errors are not removed by using the roughness model, showing that it does not perfectly account for all propagation phenomena (not only due to roughness but also to soil-water-content variability, measurement errors, calibration errors, etc.).

E. Monte Carlo Simulations

In most remote-sensing applications, ground-truth measurements are sparse. In general, only a few reference points are sampled for the estimation of the roughness parameters, and those values are then used to estimate the soil dielectric permittivity and/or water content for the rest of the area [62]. To analyze the associated uncertainty, Monte Carlo simulations were performed, whereby a certain percentage of calibration points were randomly sampled from the total ensemble of reference measurements. In our case, the percentage of calibration points varied from 1% to 100%. For each percentage, 30 independent model runs were performed with randomly chosen reference points. For all these runs, independent roughness parameters a and b were fitted following the inversion procedure shown in Fig. 3, based on the TDR measurements associated with the randomly sampled points. In the next step, these roughness parameters were used to predict ε_r of all the remaining points using the measured T_B. The rms error between radiometer-predicted and the TDR-derived ε_r was then calculated. Finally, the arithmetic mean and STD of the rms error were obtained from the 30 model runs of each percentage. The evolution of the mean and STD of the rms error with increasing percentage of calibration points is shown in Fig. 10 (note that the left ordinate is split for better visualization).

The mean rms error shows a sharp decrease with increasing number of calibration points for both polarizations, whereby the decrease is largest between 1 and ≅20%. Beyond this threshold, the mean rms error changes only slightly while approaching the value of 0.95 for the H polarization and 0.98 for the V polarization. Additionally, the STD also decreases with the increasing number of calibration points.

These results indicate that, even for a relatively homogeneous soil without any vegetation, a large number of calibration points are needed for a robust estimation of the field-scale soil water content. These results indicate that calibrating roughness parameters such as a and b for regional scales is expected to require many more ground-truth measurements than reported earlier because regional scales show a higher degree of heterogeneity in terms of soil properties (texture, structure, chemical properties, etc.) and vegetation.

IV. Summary and Conclusion

Radiometer and GPR measurements were collected over an area of 72×16 m^2 at the Selhausen test site of Forschungszentrum Jülich GmbH (Germany). As a reference ground truth, additional TDR measurements were performed within the footprints of the radiometer and the GPR. The overall moisture patterns were satisfactory reproduced by the three techniques, whereby significant differences were observed between the absolute estimations. The observed discrepancies were attributed to different sensing depths and areas and different sensitivities with respect to soil surface roughness.

For GPR, the effect of roughness was excluded by operating at low frequencies (0.2–0.8 GHz) that are not sensitive to the field surface roughness. The rms error between soil moisture measured by GPR and TDR was 0.038 $m^3 \cdot m^{-3}$. For the radiometer, the rms error significantly decreased from 0.062 (H polarization) and 0.054 (V polarization) to 0.020 $m^3 \cdot m^{-3}$

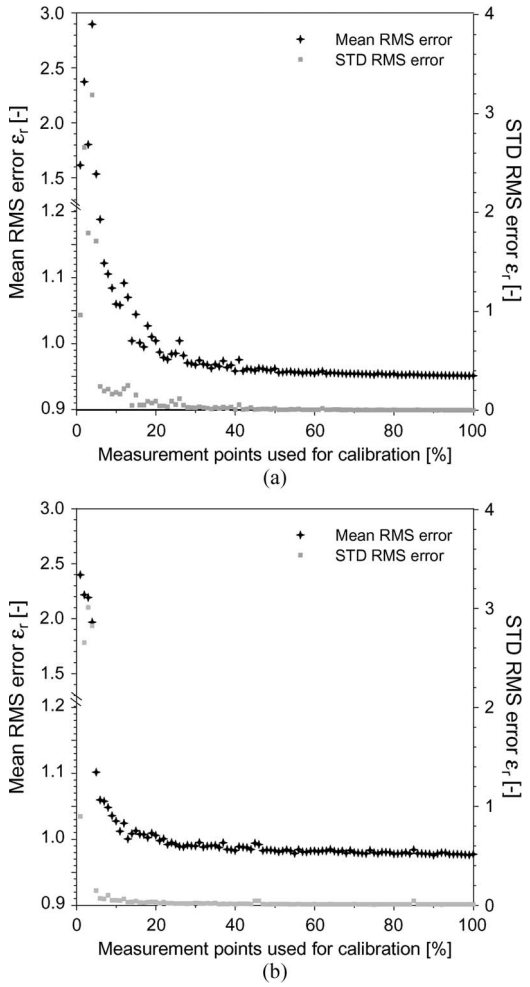

Fig. 10. RMS error with respect to the percentage of randomly sampled measurement points used for the calibration of the empirical roughness parameters a and b of (7). The mean and STD of the rms errors in terms of dielectric permittivity are estimated on the basis of 30 Monte Carlo runs (a) for H polarization and (b) for V polarization. Note that the left ordinate is split for better visualization.

(both polarizations) after accounting for roughness using an empirical model that required calibration with reference TDR measurements.

Because it is common practice in field and regional radiometer applications to estimate empirical roughness parameters on relatively small numbers of ground-truth measurements, Monte Carlo simulations were performed to estimate the associated uncertainty. These investigations showed that around 20% of the ground-truth information is required to obtain a good roughness calibration to be applied to the entire field.

This study showed that relatively accurate soil-moisture estimates were possible with L-band radiometer and off-ground GPR, although accounting for surface roughness was essential for the L-band radiometer. However, comparing different characterization techniques operating at different scales remains a difficult task in heterogeneous environments. The results of this study, in particular, provide valuable insights into the development and application of field-scale characterization techniques that could be used for improving remote-sensing data products for the retrieval of surface soil moisture. Future research will focus on the potential radiometer and GPR synergies for improving soil-moisture estimates, to be applied, for instance, in the upcoming SMAP mission.

ACKNOWLEDGMENT

The authors would like to thank Gamma Remote Sensing and Consulting AG for providing the radiometer antenna, F. André, M. Dimitrov, D. Moghadas, R. Harms, and N. Hermes of Forschungszentrum Jülich GmbH for their assistance with fieldwork, and the anonymous reviewers for their constructive comments. The JÜLBARA radiometer was funded by "Terrestrial Environmental Observatories" (TERENO) funded by the German Federal Ministry of Education and Research (BMBF).

REFERENCES

[1] A. W. Western, R. B. Grayson, and G. Bloschl, "Scaling of soil moisture: A hydrologic perspective," *Annu. Rev. Earth Planet. Sci.*, vol. 30, pp. 149–180, May 2002.

[2] F. T. Ulaby, M. K. Moore, and A. K. Fung, *Microwave Remote Sensing: Active and Passive: From Theory to Applications*, vol. III. Norwood, MA: Artech House, 1986.

[3] T. J. Jackson, J. Schmugge, and E. T. Engman, "Remote sensing applications to hydrology: Soil moisture," *Hydrol. Sci.*, vol. 41, no. 4, pp. 517–530, 1996.

[4] J. A. Huisman, S. S. Hubbard, J. D. Redman, and A. P. Annan, "Measuring soil water content with ground penetrating radar: A review," *Vadose Zone J.*, vol. 2, pp. 476–491, 2003.

[5] W. Wagner, G. Blöschl, P. Pampaloni, J. C. Calvet, B. Bizzarri, J. P. Wigneron, and Y. Kerr, "Operational readiness of microwave remote sensing of soil moisture for hydrologic applications," *Nordic Hydrol.*, vol. 38, no. 1, pp. 1–20, 2007.

[6] N. E. C. Verhoest, H. Lievens, W. Wagner, J. Alvarez-Mozos, M. S. Moran, and F. Mattia, "On the soil roughness parameterization problem in soil moisture retrieval of bare surfaces from synthetic aperture radar," *Sensors*, vol. 8, no. 7, pp. 4213–4248, Jul. 2008.

[7] Y. Oh, K. Sarabandi, and F. T. Ulaby, "An empirical-model and an inversion technique for radar scattering from bare soil surfaces," *IEEE Trans. Geosci. Remote Sens.*, vol. 30, no. 2, pp. 370–381, Mar. 1992.

[8] P. C. Dubois, J. Vanzyl, and T. Engman, "Measuring soil-moisture with imaging radars," *IEEE Trans. Geosci. Remote Sens.*, vol. 33, no. 4, pp. 915–926, Jul. 1995.

[9] J. P. Deroin, A. Company, and A. Simonin, "An empirical model for interpreting the relationship between backscattering and arid land surface roughness as seen with the SAR," *IEEE Trans. Geosci. Remote Sens.*, vol. 35, no. 1, pp. 86–92, Jan. 1997.

[10] G. D'Urso and M. Minacapilli, "A semi-empirical approach for surface soil water content estimation from radar data without a-priori information on surface roughness," *J. Hydrol.*, vol. 321, no. 1–4, pp. 297–310, Apr. 2006.

[11] T. Schmugge, P. Gloersen, T. Wilheit, and F. Geiger, "Remote-sensing of soil-moisture with microwave radiometers," *J. Geophys. Res.*, vol. 79, no. 2, pp. 317–323, 1974.

[12] T. J. Jackson, T. J. Schmugge, and J. R. Wang, "Passive microwave sensing of soil-moisture under vegetation canopies," *Water Resour. Res.*, vol. 18, no. 4, pp. 1137–1142, 1982.

[13] T. J. Jackson, D. M. Levine, C. T. Swift, T. J. Schmugge, and F. R. Schiebe, "Large-area mapping of soil-moisture using the ESTAR passive microwave radiometer in Washita'92," *Remote Sens. Environ.*, vol. 54, no. 1, pp. 27–37, Oct. 1995.

[14] T. J. Schmugge, W. P. Kustas, J. C. Ritchie, T. J. Jackson, and A. Rango, "Remote sensing in hydrology," *Adv. Water Resour.*, vol. 25, no. 8–12, pp. 1367–1385, 2002.

[15] E. G. Njoku and D. Entekhabi, "Passive microwave remote sensing of soil moisture," *J. Hydrol.*, vol. 184, no. 1/2, pp. 101–129, 1996.

[16] M. Guglielmetti, M. Schwank, C. Mätzler, C. Oberdorster, J. Vanderborght, and H. Fluhler, "Fosmex: Forest soil moisture experiments with microwave radiometry," *IEEE Trans. Geosci. Remote Sens.*, vol. 46, no. 3, pp. 727–735, Mar. 2008.

[17] J. P. Grant, A. A. Van de Griend, M. Schwank, and J. P. Wigneron, "Observations and modeling of a pine forest floor at L-band," *IEEE Trans. Geosci. Remote Sens.*, vol. 47, no. 7, pp. 2024–2034, Jul. 2009.

[18] J. S. Famiglietti, J. A. Devereaux, C. A. Laymon, T. Tsegaye, P. R. Houser, T. J. Jackson, S. T. Graham, M. Rodell, and P. J. van Oevelen, "Ground-based investigation of soil moisture variability within remote sensing footprints during the southern great plains 1997 (SGP97) hydrology experiment," *Water Resour. Res.*, vol. 35, no. 6, pp. 1839–1851, 1999.

[19] A. P. Annan, "GPR methods for hydrogeological studies," in *Hydrogeophysics*, Y. Rubin and S. Hubbard, Eds. New York: Springer-Verlag, 2005, pp. 185–213.

[20] J. R. Ernst, K. Holliger, H. Maurer, and A. G. Green, "Realistic FDTD modelling of borehole georadar antenna radiation: Methodology and application," *Near Surf. Geophys.*, vol. 4, no. 1, pp. 19–30, 2006.

[21] E. Gloaguen, B. Giroux, D. Marcotte, and R. Dimitrakopoulos, "Pseudo-full-waveform inversion of borehole GPR data using stochastic tomography," *Geophysics*, vol. 72, no. 5, pp. J43–J51, Sep./Oct. 2007.

[22] F. Soldovieri, J. Hugenschmidt, R. Persico, and G. Leone, "A linear inverse scattering algorithm for realistic GPR applications," *Near Surf. Geophys.*, vol. 5, no. 1, pp. 29–41, 2007.

[23] S. Lambot, E. C. Slob, I. van den Bosch, B. Stockbroeckx, and M. Vanclooster, "Modeling of ground-penetrating radar for accurate characterization of subsurface electric properties," *IEEE Trans. Geosci. Remote Sens.*, vol. 42, no. 11, pp. 2555–2568, Nov. 2004.

[24] L. Weihermüller, J. A. Huisman, S. Lambot, M. Herbst, and H. Vereecken, "Mapping the spatial variation of soil water content at the field scale with different ground penetrating radar techniques," *J. Hydrol.*, vol. 340, no. 3/4, pp. 205–216, Jul. 2007.

[25] S. Lambot, E. Slob, D. Chavarro, M. Lubczynski, and H. Vereecken, "Measuring soil surface water content in irrigated areas of Southern Tunisia using full-waveform inversion of proximal GPR data," *Near Surf. Geophys.*, vol. 6, pp. 403–410, 2008.

[26] P. Ferrazzoli, S. Paloscia, P. Pampaloni, G. Schiavon, D. Solimini, and P. Coppo, "Sensitivity of microwave measurements to vegetation biomass and soil-moisture content—A case-study," *IEEE Trans. Geosci. Remote Sens.*, vol. 30, no. 4, pp. 750–756, Jul. 1992.

[27] K. Saleh, J. P. Wigneron, P. Waldteufel, P. de Rosnay, M. Schwank, J. C. Calvet, and Y. H. Kerr, "Estimates of surface soil moisture under grass covers using L-band radiometry," *Remote Sens. Environ.*, vol. 109, no. 1, pp. 42–53, Jul. 2007.

[28] J. P. Wigneron, Y. Kerr, P. Waldteufel, K. Saleh, M. J. Escorihuela, P. Richaume, P. Ferrazzoli, P. de Rosnay, R. Gurney, J. C. Calvet, J. P. Grant, M. Guglielmetti, B. Hornbuckle, C. Mätzler, T. Pellarin, and M. Schwank, "L-band Microwave Emission of the Biosphere (L-MEB) model: Description and calibration against experimental data sets over crop fields," *Remote Sens. Environ.*, vol. 107, no. 4, pp. 639–655, Apr. 2007.

[29] M. Schwank, M. Guglielmetti, C. Mätzler, and H. Fluhler, "Testing a new model for the L-band radiation of moist leaf litter," *IEEE Trans. Geosci. Remote Sens.*, vol. 46, no. 7, pp. 1982–1994, Jul. 2008.

[30] B. J. Choudhury, T. J. Schmugge, and T. Mo, "A parameterization of effective soil-temperature for microwave emission," *J. Geophys. Res.*, vol. 87, no. C2, pp. 1301–1304, 1982.

[31] A. Chanzy, S. Raju, and J. P. Wigneron, "Estimation of soil microwave effective temperature at L and C bands," *IEEE Trans. Geosci. Remote Sens.*, vol. 35, no. 3, pp. 570–580, May 1997.

[32] B. J. Choudhury, T. J. Schmugge, A. Chang, and R. W. Newton, "Effect of surface-roughness on the microwave emission from soils," *J. Geophys. Res.*, vol. 84, no. C9, pp. 5699–5706, 1979.

[33] T. Mo and T. J. Schmugge, "A parameterization of the effect of surface-roughness on microwave emission," *IEEE Trans. Geosci. Remote Sens.*, vol. GRS-25, no. 4, pp. 481–486, Jul. 1987.

[34] C. Mätzler, "Passive microwave signatures of landscapes in winter," *Meteorol. Atmos. Phys.*, vol. 54, no. 1–4, pp. 241–260, Mar. 1994.

[35] C. Mätzler and A. Standley, "Relief effects for passive microwave remote sensing," *Int. J. Remote Sens.*, vol. 21, no. 12, pp. 2403–2412, 2000.

[36] T. J. Jackson, "Measuring surface soil-moisture using passive microwave remote-sensing," *Hydrol. Process.*, vol. 7, no. 2, pp. 139–152, 1993.

[37] J. P. Wigneron, A. Chanzy, J. C. Calvet, and W. Bruguier, "A simple algorithm to retrieve soil-moisture and vegetation biomass using passive microwave measurements over crop fields," *Remote Sens. Environ.*, vol. 51, no. 3, pp. 331–341, Mar. 1995.

[38] H. Vereecken, J. A. Huisman, H. Bogena, J. Vanderborght, J. A. Vrugt, and J. W. Hopmans, "On the value of soil moisture measurements in vadose zone hydrology: A review," *Water Resour. Res.*, vol. 44, p. W00D06, Oct. 2008.

[39] S. Lambot, L. Weihermüller, J. A. Huisman, H. Vereecken, M. Vanclooster, and E. C. Slob, "Analysis of air-launched ground-penetrating radar techniques to measure the soil surface water content," *Water Resour. Res.*, vol. 42, p. W11403, 2006, DOI: 11410.11029/12006WR005097.

[40] T. J. Heimovaara and W. Bouten, "A computer-controlled 36-channel time domain reflectometry system for monitoring soil water contents," *Water Resour. Res.*, vol. 26, no. 10, pp. 2311–2316, 1990.

[41] D. A. Robinson, M. G. Schaap, D. Or, and S. B. Jones, "On the effective measurement frequency of time domain reflectometry in dispersive and nonconductive dielectric materials," *Water Resour. Res.*, vol. 41, no. 2, p. W02007, Feb. 2005.

[42] C. Mätzler, D. Weber, M. Wuthrich, K. Schneeberger, C. Stamm, H. Wydler, and H. Fluhler, "ELBARA, the ETH L-band radiometer for soil-moisture research," in *Proc. 23rd IGARSS*, Toulouse, France, 2003, pp. 3058–3060.

[43] T. Pellarin, J. P. Wigneron, J. C. Calvet, M. Berger, H. Douville, P. Ferrazzoli, Y. H. Kerr, E. Lopez-Baeza, J. Pulliainen, L. P. Simmonds, and P. Waldteufel, "Two-year global simulation of L-band brightness temperatures over land," *IEEE Trans. Geosci. Remote Sens.*, vol. 41, no. 9, pp. 2135–2139, Sep. 2003.

[44] K. A. Michalski and J. R. Mosig, "Multilayered media green's functions in integral equation formulations," *IEEE Trans. Antennas Propag.*, vol. 45, no. 3, pp. 508–519, Mar. 1997.

[45] E. C. Slob and J. Fokkema, "Coupling effects of two electric dipoles on an interface," *Radio Sci.*, vol. 37, no. 5, p. 1073, Sep. 2002, DOI: 1010.1029/2001RS002529.

[46] S. Lambot, M. Antoine, M. Vanclooster, and E. C. Slob, "Effect of soil roughness on the inversion of off-ground monostatic GPR signal for noninvasive quantification of soil properties," *Water Resour. Res.*, vol. 42, p. W03403, 2006, DOI: 03410.01029/02005WR004416.

[47] J. P. Wigneron, L. Laguerre, and Y. H. Kerr, "A simple parameterization of the L-band microwave emission from rough agricultural soils," *IEEE Trans. Geosci. Remote Sens.*, vol. 39, no. 8, pp. 1697–1707, Aug. 2001.

[48] F. T. Ulaby, M. K. Moore, and A. K. Fung, *Microwave Remote Sensing: Active and Passive: Fundamentals and Radiometry*, vol. I. Boston, MA: Addison Wesley, 1981.

[49] J. A. Kong, *Electromagnetic Wave Theory*, 2nd ed. New York: Wiley, 1990.

[50] J. R. Wang and B. J. Choudhury, "Remote-sensing of soil-moisture content over bare field at 1.4 GHz frequency," *J. Geophys. Res.*, vol. 86, no. C6, pp. 5277–5282, 1981.

[51] E. G. Njoku, T. J. Jackson, V. Lakshmi, T. K. Chan, and S. V. Nghiem, "Soil moisture retrieval from AMSR-E," *IEEE Trans. Geosci. Remote Sens.*, vol. 41, no. 2, pp. 215–229, Feb. 2003.

[52] J. C. Shi, K. S. Chen, Q. Li, T. J. Jackson, P. E. O'Neill, and L. Tsang, "A parameterized surface reflectivity model and estimation of bare-surface soil moisture with L-band radiometer," *IEEE Trans. Geosci. Remote Sens.*, vol. 40, no. 12, pp. 2674–2686, Dec. 2002.

[53] M. Schwank, I. Volksch, J. P. Wigneron, Y. H. Kerr, A. Mialon, P. de Rosnay, and C. Matzler, "Comparison of two bare-soil reflectivity models and validation with L-band radiometer measurements," *IEEE Trans. Geosci. Remote Sens.*, vol. 48, no. 1, pp. 325–337, Jan. 2010.

[54] M. Schwank and C. Mätzler, "Modelling the soil microwave emission," in *Thermal Microw. Radiat.: Appl. Remote Sens.*, C. Mätzler, Ed. London, U.K.: Inst. Eng. Technol., 2006, pp. 287–301.

[55] M. J. Escorihuela, Y. H. Kerr, P. de Rosnay, J. P. Wigneron, J. C. Calvet, and F. Lemaitre, "A simple model of the bare soil microwave emission at L-band," *IEEE Trans. Geosci. Remote Sens.*, vol. 45, no. 7, pp. 1978–1987, Jul. 2007.

[56] M. J. Escorihuela, A. Chanzy, J. P. Wigneron, and Y. H. Kerr, "Effective soil moisture sampling depth of L-band radiometry: A case study," *Remote Sens. Environ.*, vol. 114, no. 5, pp. 995–1001, May 2010.

[57] S. Lambot, E. C. Slob, I. van den Bosch, B. Stockbroeckx, B. Scheers, and M. Vanclooster, "Estimating soil electric properties from monostatic ground-penetrating radar signal inversion in the frequency domain," *Water Resour. Res.*, vol. 40, p. W04205, Apr. 2004, DOI: 04210.01029/02003WR002095.

[58] G. Topp, J. L. Davis, and A. P. Annan, "Electromagnetic determination of soil water content: Measurements in coaxial transmission lines," *Water Resour. Res.*, vol. 16, no. 3, pp. 574–582, 1980.

[59] A. Chanzy, A. Tarussov, A. Judge, and F. Bonn, "Soil water content determination using digital ground penetrating radar," *Soil Sci. Soc. Amer. J.*, vol. 60, pp. 1318–1326, 1996.

[60] J. Minet, S. Lambot, E. C. Slob, and M. Vanclooster, "Soil surface water content estimation by full-waveform GPR signal inversion in the presence of thin layers," *IEEE Trans. Geosci. Remote Sens.*, vol. 48, no. 3, pp. 1138–1150, Mar. 2010.
[61] T. Mo, T. J. Schmugge, and J. R. Wang, "Calculations of the microwave brightness temperature of rough soil surfaces: Bare field," *IEEE Trans. Geosci. Remote Sens.*, vol. GRS-25, no. 1, pp. 47–54, Jan. 1987.
[62] R. Panciera, J. P. Walker, J. D. Kalma, E. J. Kim, K. Saleh, and J. P. Wigneron, "Evaluation of the SMOS L-MEB passive microwave soil moisture retrieval algorithm," *Remote Sens. Environ.*, vol. 113, no. 2, pp. 435–444, Feb. 2009.
[63] K. Z. Jadoon, E. Slob, H. Vereecken, and S. Lambot, "Analysis of horn antenna transfer functions and phase-center position for modeling off-ground GPR," *IEEE Trans. Geosci. Remote Sens*, vol. 49, no. 5, pp. 1649–1662, May 2011.

François Jonard received the Eng. and M.Sc. degrees in environmental engineering from the Université Catholique de Louvain (UCL), Louvain-la-Neuve, Belgium, in 2002. He is currently working toward the Ph.D. degree in hydrogeophysics and microwave remote sensing (active and passive) in the Institute of Bio- and Geosciences, Forschungszentrum Jülich GmbH, Jülich, Germany.

In the past years, he has gained experience in forest hydrology modeling, working as a Research Assistant with the Earth and Life Institute, UCL. From 2005 to 2009, he was a Consultant with the European Commission in the fields of geographic information systems and remote sensing applied to environmental issues. His research interests particularly focus on soil-moisture retrieval with ground-penetrating radar and microwave radiometry forward and inverse modeling.

Lutz Weihermüller received the Diploma degree in geography from the University Bremen, Bremen, Germany, and the Ph.D. degree in numerical modeling from the University of Bonn, Bonn, Germany, in 2005.

He is currently a Postdoc with the Forschungszentrum Jülich GmbH, Jülich, Germany. His research interests are numerical modeling of water, solute, and gas transports in the unsaturated zone and parameter estimation for various applications. In addition, he works on different hydrogeophysical methods such as ground-penetrating radar and radiometry for soil water monitoring.

Dr. Weihermüller is a member of the American Geophysical Union, European Geosciences Union, and Soil Science Society of America.

Khan Zaib Jadoon received the M.Sc. degree in geophysics from the Quaid-i-Azam University, Islamabad, Pakistan, in 2006 and the Ph.D. degree in ground-penetrating radar applied to agricultural and environmental issues from the Université Catholique de Louvain, Louvain-la-Neuve, Belgium.

He is currently a Postdoc Researcher with the Institute of Bio- and Geosciences, Forschungszentrum Jülich GmbH, Jülich, Germany. His research interests particularly focus on soil hydraulic property estimation at the field scale from integrated hydrogeophysical inversion of time-lapse full-waveform ground-penetrating-radar data.

Dr. Jadoon is a member of the American Geophysical Union, European Geosciences Union, Society of Exploration Geophysicists, and International Glaciological Society.

Mike Schwank received the Ph.D. degree in physics from the Swiss Federal Institute of Technology (ETH), Zürich, Switzerland, in 1999. The topic of his Ph.D. thesis was "nanolithography using a high-pressure scanning-tunneling microscope."

In the following three years, he gained experience in the industrial environment, where he was a Research and Development Engineer in the field of micro-optics. In 2003, he started working in the research field of microwave remote sensing applied to soil-moisture detection. Until 2010, he was a Senior Research Assistant with the Swiss Federal Institute for Forest, Snow and Landscape Research (WSL), Birmensdorf, Switzerland. His research involved practical and theoretical aspects of microwave radiometry. In addition to his research at WSL, he was also with the company Gamma Remote Sensing Research and Consulting AG, Gümligen, Switzerland, where he was involved in the production of microwave radiometers to be deployed for ground-based Soil Moisture and Ocean Salinity calibration/validation purposes. Currently, he is with the German Research Centre for Geosciences GFZ, Potsdam, Germany, where he is in charge of the coordination of the Terrestrial Environmental Observatories (TERENO)'s Northeastern Lowland observatory in Germany.

Harry Vereecken received the Eng. and M.Sc. degrees in agricultural engineering and the Ph.D. degree in agricultural sciences from the Katholieke Universiteit Leuven, Leuven, Belgium, 1982 and 1988, respectively. His Ph.D. was on the development of pedotransfer functions to estimate soil hydraulic properties.

From 1988 to 1990, he was a Research Assistant, working on modeling nitrogen and water fluxes in soils and groundwater. From 1990 to 1992, he was Researcher with the Institute for Petroleum and Organic Geochemistry, Forschungszentrum Jülich GmbH (FZJ), Jülich, Germany, where he became the Head of the division on "behavior of pollutants in geological systems" from 1992 to 2000. He was appointed Director of the Agrosphere (IBG-3), Institute of Bio- and Geosciences, FZJ, in 2000. His current field of research is modeling of flow and transport processes in soils and hydrogeophysics.

Sébastien Lambot received the Eng. and M.Sc. degrees in agricultural engineering and the Ph.D. degree (*summa cum laude*) in engineering sciences from the Université Catholique de Louvain (UCL), Louvain-la-Neuve, Belgium, in 1999 and 2003, respectively.

In 2004–2005, he was with The Delft University of Technology, Delft, The Netherlands, as a European Marie Curie Fellow. In 2006, he was with Forschungszentrum Jülich GmbH (FZJ), Jülich, Germany, as Research Group Leader. He is currently an Associate Professor and a Fonds de la Recherche Scientifique Research Associate with UCL and partly works with FZJ. His current research interests include hydrogeophysics, ground-penetrating radar and electromagnetic interference forward and inverse modeling and digital soil mapping over different scales. He published more than 35 journal papers on these subjects. He is an Associate Editor for *Vadose Zone Journal* and was a Guest Editor of two special issues on hydrogeophysics.

Dr. Lambot was the General Chair of the 3rd International Workshop on Advanced Ground Penetrating Radar in 2005 and organized several hydrogeophysics sessions in international conferences.